RESEARCH PAPER

Synthesis of Polythiophene/Manganese Dioxide Nanocomposites by *In-situ* Core-shell Polymerization Method and Study of their Physical Properties

Sina Khanmohammadi, Mirzaagha Babazadeh*

Department of Chemistry, Tabriz Branch, Islamic Azad University, Tabriz, Iran

ARTICLE INFO

ABSTRACT

The present research work describes an efficient method for facile synthesis of α-MnO$_2$ nanorods by hydrothermal method and preparation of a series of polythiophene/manganese dioxide (PTh/MnO$_2$) nanocomposites with various α-MnO$_2$ ratios. These nanocomposites were fabricated by *in-situ* oxidative polymerization method using FeCl$_3$ as oxidant, and characterized by Fourier transformed infrared (FT-IR), X-ray diffraction (XRD), energy-dispersive X-ray (EDX), thermogravimetric thermal analyses (TGA), scanning electron microscopy (SEM) and transmission electron microscopy (TEM) techniques. FT-IR, EDX and XRD data showed that as-synthesized α-MnO$_2$ nanorods has been definitely incorporated into the polymer matrix *via in-situ* core-shell polymerization. SEM and TEM pictures showed that the nanocomposites have rod-like morphology with the average diameter of 50-70 nm. TGA measurements showed that introducing α-MnO$_2$ nanorods into PTh matrix, improve the thermal stability of nanocomposites in comparison with pure PTh. This employed method is very simple and inexpensive in comparison with methods applied by other researchers, and it can be easily applied industrially.

INTRODUCTION

Conducting polymers such as polyaniline (PANI), polypyrrole (PPy) and polythiophene (PTh) with extensive π-electron delocalization along their backbones are considered to be the most important semiconducting materials because of their fascinating chemical and physical properties useful for various applications [1,2]. These materials may combine the process ability and outstanding mechanical characteristics of polymers with the readily-tailored electrical, optical, and magnetic properties of functional organic molecules. In particular, the potential use of these materials in light-emitting diodes [3], field-effect transistors [4], photovoltaic cells [5], and other opto-electronic devices has motivated the development of synthesis and processing methods of conjugated polymer materials with unique properties [6].

PTh and its derivatives have attracted much consideration because of their easy preparation, environmental stability, higher conductivity and photoconduction [7,8]. PTh is produced from the polymerization of thiophene, as a sulphur heterocycle, by connecting thiophene through its 2,5 positions. Three approaches to polymerization of thiophene have been reported in the literature: (1) electropolymerization, (2) metal-catalyzed coupling reactions, and (3) chemical oxidative polymerization [9]. When PTh was combined with different inorganic materials such as metal or metal oxide nanoparticles, it produced nano-composite materials. Nanocomposites are the special class of materials which exhibit unique physical, chemical and biological properties [10]. The investigation of polymer-inorganic nanocomposites is motivated by many reasons, including the need for novel electronic anisotropic

* Corresponding Author Email: babazadeh@iaut.ac.ir

materials [11], better performing battery [12], cathode materials [13], functional structural materials with superior mechanical and thermal properties [14]. It is expected that the uses of new functional inorganic nano-fillers will lead to new polymer-inorganic nanocomposites with unique combinations of material properties. In the recent years, synthesis and application of conducting polymers nanocomposites with various inorganic nanoparticles such as CdS [15], NiO [16], SnO_2 [17], SiO_2 [18], V_2O_5 [19], CuO [20], Cu_2O [21], Al_2O_3 [22], ZnO [23], Fe_3O_4 [24], and TiO_2 [25] have been reported.

In recent years, manganese dioxide (MnO_2) has attracted enormous attentions due to its physical and chemical properties such as low cost, abundant availability, high surface area, adsorption ability, good stability under acidic conditions and environmental compatibility [26]. The MnO_2 has been widely used in wastewater treatment [27], molecular/ion sieves [28] and electrode materials in batteries or capacitors [29] because of its different and unique structures. MnO_2 exists in several crystallographic forms, such as α-, β-, γ-, δ-, λ- and ε-type, when the basic unit [MnO_6] octahedron links in different ways [30]. Among these crystallographic forms, 1D α-MnO_2 nanorods have received special attention as cathodic materials for lithium batteries since the large tunnels existing in the crystalline lattice of α-MnO_2 are believed to facilitate the accommodation and transportation of inserting lithium ions [31]. So far, numerous efforts have been devoted to synthesize MnO_2 nanostructures and a variety of strategies have been developed, including thermal decomposition, coprecipitation [32], simple reduction [33], hydrothermal method [34], sol-gel [35] and etc. Among these methods, hydrothermal synthesis has attracted more attention for preparation of nanostructured materials such as metal oxides, chalcogenides, and metals because it is easily controlled on the shape of materials, which are simple processed and in large scale [36-38].

This paper reports the controlled synthesis of α-MnO_2 nanostructures *via* a facile hydrothermal route without using any physical template and addition of any surfactant. α-MnO_2 nanorods was synthesized based on the hydrothermal reaction of $MnSO_4$ and $KMnO_4$ in aqueous medium. Then, a novel serious of PTh/MnO_2 nanocomposites was synthesized by one step *in-situ* polymerization of thiophene in the presence of different amounts of α-MnO_2 nanorods. The characteristics of the molecular structure, crystallinity, thermal stability, and morphology of the PTh/MnO_2 nanocomposites are also discussed. Therefore, synthesis of a new serious of PTh/MnO_2 nanocomposites for the first time and studying their physical properties are the main novelty of this work.
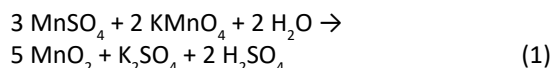
MATERIALS AND METHODS
Materials
Thiophene was purchased from Mreck and distilled to obtain a colorless liquid. Then was kept below 4°C. Chloroform was purchased from Merck and dried by standard procedure before use. Anhydrous $FeCl_3$, $MnSO_4.H_2O$, $KMnO_4$ and other reagents were provided from Merck and used as received. All chemical used were of analytical grade and double distilled water was used for solution preparation.

Preparation of α-MnO_2 nanorods
α-MnO_2 nanorods were produced by the hydrothermal reaction [39, 40]. In a typical synthesis, $MnSO_4.H_2O$ (1.69 g, 0.1 mol) and $KMnO_4$ (3.16 g, 0.2 mol) were mixed in the distilled water at room temperature and magnetically stirred to form a homogeneous mixture. When the mixed solution changed to a dark brown gel-like solution, it was immediately transferred into a Teflon-lined stainless steel autoclave and heated at 140°C for 12 h. After the reaction was complete, the reactor was taken out and naturally cooled to room temperature. The resulting brownish-black solid product was filtered off, washed with distilled water to remove ions possibly remaining in the final products, and finally dried at 120°C in air overnight. The production yield of α-MnO_2 nanorods was about 92% based on Manganese quantity in the starting reagents. The chemical reaction is shown in Eq. (1).

$$3\ MnSO_4 + 2\ KMnO_4 + 2\ H_2O \rightarrow$$
$$5\ MnO_2 + K_2SO_4 + 2\ H_2SO_4 \qquad (1)$$

Preparation of PTh/MnO_2 nanocomposites
The PTh/MnO_2 nanocomposites were chemically synthesized by *in-situ* oxidative polymerization of thiophene using $FeCl_3$ as oxidant under controlled conditions. As-synthesized α-MnO_2 in different weight percentage (5%, 10%, 15% and 20%) was dispersed in flask containing 50 ml of dry $CHCl_3$ and

thiophene (1 g, 48 mmol) was then added into the flask. The mixture was sonicated in an ultrasound bath for 20 minutes to get well dispersed. Then, anhydrous $FeCl_3$ (7.8 g, 48 mmol) was dissolved in 50 ml of dry $CHCl_3$ and added dropwise into the mixture at room temperature. The *in-situ* polymerization was started immediately and continued for 24 h at room temperature. The dark gray precipitate was recovered by filtration and extracted with methanol for 24 h to remove of the residual $FeCl_3$ and unreacted monomer. During this procedure, the color of nanocomposites changed from black (PTh in oxide state) to red brown (PTh in reduced state), which indicated the successful reduction of PTh shell. A series of PTh/MnO_2 nanocomposites designated as PTh/MnO_2 (5%), PTh/MnO_2 (10%), PTh/MnO_2 (15%), and PTh/MnO_2 (20%) was obtained in high yield (75-90%) after washing with methanol for several times and drying at 80°C for 3 h in vacuum oven.

Pure PTh was prepared applying above procedure in the absence of α-MnO_2 nanoparticles.

Instrumental measurements

FT-IR spectra were recorded on a Bruker Spectrometer Tensor 27 FTIR with KBr pellets. X-ray diffraction (XRD) patterns of α-MnO_2, PTh, and PTh/MnO_2 nanocomposites were measured in the range of 2ϴ=10-70° by step scanning on the Siemens X-ray diffraction D5000 with Cu Kα radiation (λ=0.154 nm). The elements of samples were measured on energy-dispersive X-ray (EDX) spectroscopy, which was taken on a Leo1430VP microscope with operating voltage 5 kV. The process of EDX measures were carried out with a pellet which was pressed at 200 MPa and then adhered to copper platens. The morphology of

α-MnO_2, PTh, and PTh/MnO_2 nanoparticles was investigated by scanning electron microscopy (SEM, LEO-440i). The size of particles was investigated with a Hitachi 600 transmission electron microscope (TEM). Thermal stability of α-MnO_2, pure PTh and nanocompistes was investigated by thermal gravimetric analyzer (Perkin Elmer, TGA-7) under a nitrogen flow (35 ml/min) and heating rate of 10°C/min.

RESULTS AND DISCUSSION

Thiophene and its derivatives can be polymerized by both chemical and electrochemical methods. Chemical method is preferred over electrochemical methods because of its simplicity and scalability. For many years, oxidative polymerization method using $FeCl_3$ had been the synthetic inexpensive method of choice for the preparation of PTh. Thiophene is not stable in protic acid media, therefore, $FeCl_3$ as a Lewis acid in dry $CHCl_3$ is used as oxidant [41]. Fig. 1 shows the proposed mechanism for thiophene oxidative polymerization. The active sites in the polymerization are the crystal Fe^{3+} surface ions. They have one unshared chloride and one empty orbital, which is the source of their Lewis acidity. The soluble part of $FeCl_3$ is inert because it exists in a dimeric form without empty orbitals. The reaction starts by complexation between the thiophene sulfur and the $FeCl_3$ to form a cation radical, which upon deprotonation yields the initiating radical. The mechanism also proposes that the combination of thiophene radicals gives mainly the 2,5-disubstituted thiophene moieties in the PTh chains. The effective reaction needs a 4:1 mole ratio of $FeCl_3$: thiophene. This requirement is because the polymerization process requires
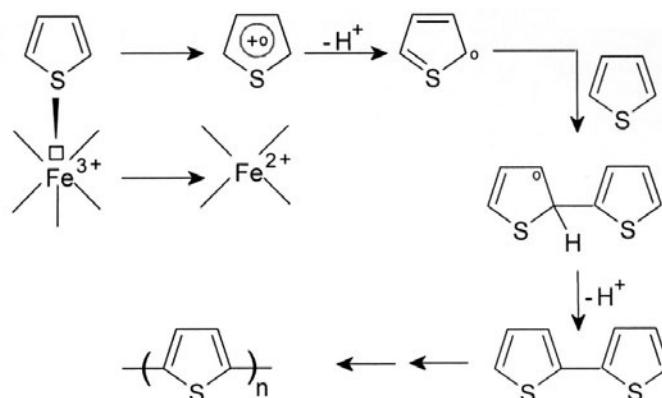

Fig. 1. Proposed mechanism of thiophene oxidative polymerization with $FeCl_3$ in $CHCl_3$.

solid $FeCl_3$, and 50% of the $FeCl_3$ dissolves in the $CHCl_3$ [42]. In addition, the HCl byproduct consumes $FeCl_3$ to form the $FeCl_4^-$ complex ion. Homopolymerization also takes place in this reaction mixture, yielding a reddish PTh powder after dedoping with methanol.

Study of FT-IR spectroscopy results

The FT-IR spectra of the PTh, and PTh/MnO$_2$ nanocomposites are shown in Fig. 2. The band at around 3500 cm^{-1} corresponds to the O-H vibrating mode of traces of absorbed water. In the FT-IR spectrum of pure PTh, the several low-intensity absorption peaks at 2800-3100 cm^{-1} can be attributed to the aromatic C-H stretching vibration bands. The bans at 1565 and 1400 cm^{-1} were ascribed to the C=C asymmetric and symmetric stretching vibrations of thiophene ring, respectively. The absorption peak at 784 cm^{-1} was ascribed to the =C-H out of plane vibration of α,α'-coupling of poly-2,5-thiophene which confirmed

the polymerization of thiophene monomer. The peaks at 1200 and 1040 cm^{-1} were due to C-H bending and C-H in-plane deformation. The absorption peak at 684 cm^{-1} was assigned to the C-S bending mode, which indicated the presence of thiophene monomer [43]. The PTh/MnO$_2$ nanocomposites spectrum shows nearly identical numbers and positions of the pure PTh bands. The C-H stretching vibrations and C=C characteristic peaks can be identified almost in the same range at 2800-3100 cm^{-1} and 1590 cm^{-1}, respectively. The band located at 500 cm^{-1} can be ascribed to the Mn-O stretching vibration of MnO$_2$ nanopowder [44]. The peak at 830 cm^{-1} should be ascribed to the C-H out of plane stretching vibration mode of PTP.

Study of XRD patterns

The X-ray diffraction (XRD) patterns of the pure PTh and PTh/MnO$_2$ nanocomposites are shown in Fig. 3. The broad peak in the region of 2θ=25°
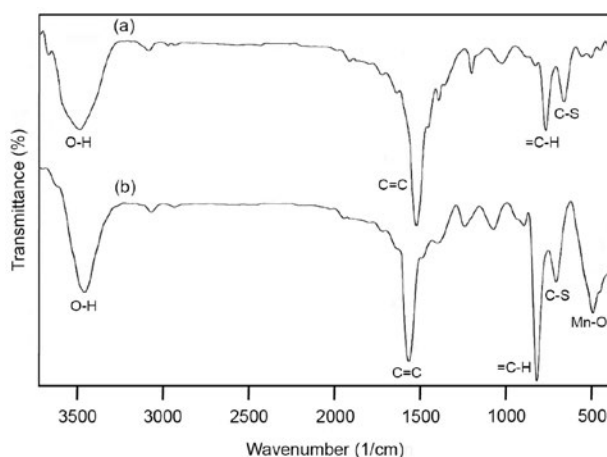

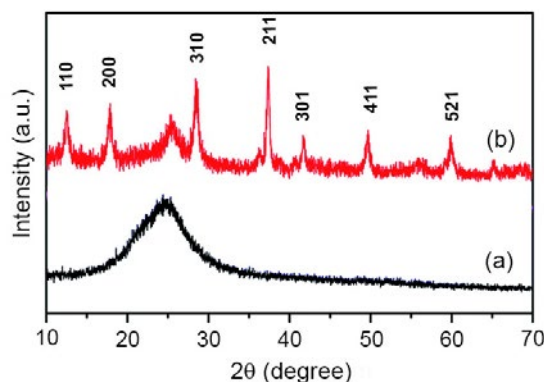Fig. 2. FT-IR spectra of (a) pure PTh and (b) PTh/MnO$_2$ nanocomposites.

Fig. 3. XRD pattern of (a) pure PTh and (b) PTh/MnO$_2$ (20%) nanocomposite.

in XRD pattern of pure PTh (Fig. 3a) shows that the synthesized PTh in the absence of α-MnO$_2$ nanorods is amorphous. The XRD pattern of the PTh/MnO$_2$ nanocomposites (Fig. 3b) shows strong sharp diffraction peaks at 12.7°(110), 18.1°(200), 28.8°(310), 37.4°(211), 49.8°(411), 60.2°(521) can be indexed to tetragonal phase of α-MnO$_2$ (JCPDS Card, No.44-0141) [45]. In addition, no diffraction peaks for impurities are observed, which suggests the high purity of the product. As shown in Fig. 3b, the broad diffraction peak around $2\vartheta=25°$ which is caused by the periodicity perpendicular to the polymer chains of PTh still exists, but its intensity has been decreased. This means that PTh deposited on the surface of α-MnO$_2$ nanorods has no effect on the crystallization of α-MnO$_2$, and each phase maintains his initial structure.

The average crystallite size of as-synthesized α-MnO$_2$ nanorods and PTh/MnO$_2$ nanocomposites is calculated by Scherrer formula (Eq. 2) [46-48]:
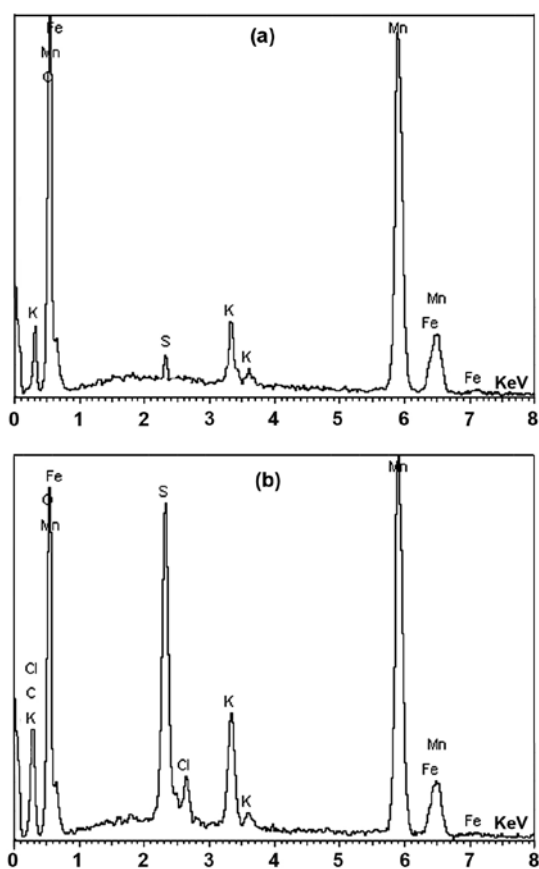
$$D = K\lambda/\beta \cos\Theta \qquad (2)$$

Fig. 4. EDX spectra of (a) α-MnO$_2$ nanorods and (b) PTh/MnO$_2$ (20%) nanocomposite.

where D is crystallite size of particle, λ is X-ray wavelength (0.154 nm for Cu-Kα), K is the shape factor, which can be assigned a value of 0.89 if the shape is unknown, Θ is Bragg diffraction angle and β is the full width at half-height of angle of diffraction in radians. The above equation was introduced for the characteristic (211 plane) peak at $2\Theta=37.4°$. The obtained results showed that the average particle size of α-MnO$_2$ nanorods and PTh/MnO$_2$ nanocomposites was 37 nm and 50-70, respectively. These results were in good agreement with the TEM and SEM images.

Study of EDX spectroscopies

The EDX spectra of as-synthesized α-MnO$_2$ and PTh/MnO$_2$ (20%) nanocomposite are shown in Fig. 4. It was found that the major elements of as-synthesized α-MnO$_2$ are Mn and O. (Fig. 4a). A small amount of Fe was possibly contaminated by instrumentation (autoclave). In EDX spectrum of PTh/MnO$_2$ nanocomposites (Fig. 4b), the major elements are Mn, O, S and C. This further proves that the PTh/MnO$_2$ nanocomposites are synthesized successfully. Furthermore, the element of Cl and Fe are observed in nanocomposites, which should be resulted from FeCl$_3$ which used as an oxidant in polymerization.

Study of SEM and TEM pictures

Fig. 5 shows representative TEM image of the as-synthesized α-MnO$_2$. The as-synthesized α-MnO$_2$ contains 100% rod-like morphology with smooth surface and no other morphology has been detected. TEM image shows that diameter of the α-MnO$_2$ nanorods is in the range of 30-40 nm and the length is about 0.5 μm.

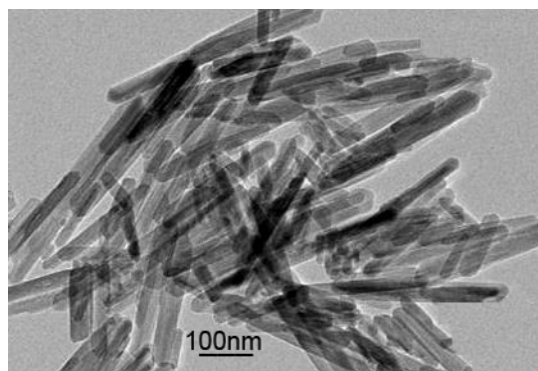SEM technique was performed to investigate the dimensions and the morphology of PTh/

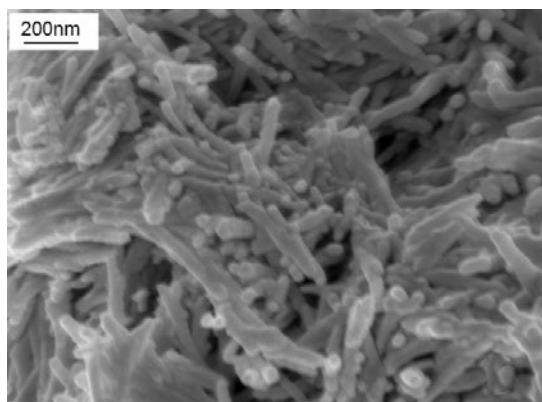Fig. 5. TEM photograph of α-MnO$_2$ nanorods.

Fig. 6. SEM image of PTh/MnO$_2$ (20%) nanocomposite.

MnO$_2$ nanocomposites. A typical SEM image of PTh/MnO$_2$ (20%) nanocomposite is shown in Fig. 6. The nanocomposite has rod-like morphology with average diameter of 50-70 nm which are linked together. In nanocomposites, the thiophene monomers are adsorbed onto the surface of α-MnO$_2$ nanorods due to the electrostatic interaction. Thus, the polymerization has a preferring trend on the surfaces of MnO$_2$.

Study of thermal stability

The thermal stability behavior of α-MnO$_2$ nanoparticles, pure PTh and PTh/MnO$_2$ nano-composites were investigated by the thermal gravimetric analyzer in the temperature range of 20-800°C (Fig. 7). The neat α-MnO$_2$ is stable and shows a trace weight change in the whole investigated temperature range (Fig. 7a). Around 5% weight loss in α-MnO$_2$ nanorods is observed up to the temperature 250°C, which can be attributed

to the removal of physically adsorbed water. There is a 6% weight loss between 550 and 650°C, which can be ascribed to the reduction of manganese from tetravalent to trivalent form accompanied by the evolution of oxygen [49].

TGA diagram of pure PTh (Fig. 7b) shows three major stages of weight loss. The first loss weight in the range of 20-140°C can be attributed to the evolution of water molecules. The second stage, in the temperature range of 140-320°C, is related to removal of dopant anions from the polymer structure. The last weight loss observed between 320-650°C corresponds to the degradation of the PTh polymer chains. At the ending temperature of 800°C, the weight loss of the pure PTh is 96%.

Study of TGA diagram of PTh/MnO$_2$ (20%) nanocomposite (Fig. 7c) shows that PTh/MnO$_2$ nanocomposite is stable up to 400°C, and decomposes completely at 650°C. At the ending temperature of 800°C, the weight loss of PTh/ MnO$_2$ (20%) nanocomposite is 63%. The obtained results indicate that introduction of α-MnO$_2$ nanoparticles into PTh polymer matrix increases the thermal stability of PTh around 33%. As a result, these data confirm that the presence of α-MnO$_2$ nanoparticles in the PTh/MnO$_2$ nanocomposites is responsible for the high thermal stability of the synthesized nanocomposites in comparison with pure PTh.

CONCLUSION

In summary, α-MnO$_2$ nanorods were prepared with hydrothermal precipitation method at 140°C for 12 h. Then, a novel serious of PTh/ MnO$_2$ nanocomposites was synthesized by one-
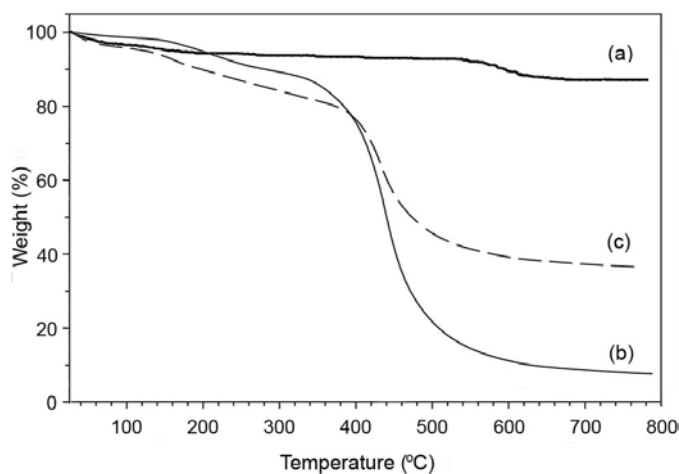

Fig. 7. TGA diagrams of (a) α-MnO$_2$, (b) PTh and (c) PTh/MnO$_2$ (20%) nanocomposite.

step *in-situ* chemical oxidative polymerization of thiophene containing different weight percentage of as-prepared α-MnO$_2$ nanorods. The FT-IR and EDX spectra showed presence and encapsulation of α-MnO$_2$ in the PTh matrix. The XRD study revealed that PTh deposited on the surface of α-MnO$_2$ nanoparticles has no effect on the crystallization of α-MnO$_2$, and each phase maintains his initial structure. SEM and TEM images of PTh/MnO$_2$ nanocomposites showed strong effect of α-MnO$_2$ nanoparticles on the morphology of nanocomposites. PTh/MnO$_2$ nanocomposites had rod-like morphology similar to α-MnO$_2$ morphology. TGA plots showed that the synthesized PTh/MnO$_2$ nanocomposites had higher thermal stability in comparison with pure PTh. Finally, the employed method is very simple and inexpensive in comparison with other applied methods, and it can be easily applied industrially.

CONFLICT OF INTEREST

The authors declare that there are no conflicts of interest regarding the publication of this manuscript.

REFRENCES

1. Babazadeh M, Sheidaei M, Sattary S. Investigation of Structural, Thermal, and Electrical Properties of Nanocomposites Based on SnO2Nanoparticles Dispersed in Conducting Polypyrrole Matrix. Synthesis and Reactivity in Inorganic, Metal-Organic, and Nano-Metal Chemistry. 2014;44(6):819-24.

2. Babazadeh M, Rezazad Gohari F, Olad A. Characterization and physical properties investigation of conducting polypyrrole/TiO2 nanocomposites prepared through a one-step "in situ" polymerization method. Journal of Applied Polymer Science. 2011;123(4):1922-7.

3. Kim M, Lee YS, Kim YC, Choi MS, Lee JY. Flexible organic light-emitting diode with a conductive polymer electrode. Synthetic Metals. 2011;161(21-22):2318-22.

4. Chauhan AK, Gupta SK, Taguchi D, Manaka T, Jha P, Veerender P, et al. Enhancement of the carrier mobility of conducting polymers by formation of their graphene composites. RSC Advances. 2017;7(20):11913-20.

5. Liu R. Hybrid Organic/Inorganic Nanocomposites for Photovoltaic Cells. Materials. 2014;7(4):2747-71.

6. Wang G, Zhang L, Zhang J. A review of electrode materials for electrochemical supercapacitors. Chem Soc Rev. 2012;41(2):797-828.

7. Ansari MO, Khan MM, Ansari SA, Cho MH. Polythiophene nanocomposites for photodegradation applications: Past, present and future. Journal of Saudi Chemical Society. 2015;19(5):494-504.

8. khezri T, Sharif M, Pourabas B. Polythiopheneâ€"graphene oxide doped epoxy resin nanocomposites with enhanced electrical, mechanical and thermal properties. RSC Advances. 2016;6(96):93680-93.

9. Rusen E, Diacon A, Mocanu A, GavrilÄ́f R, Nistor LC, Dinescu A. CdSe (quantum dots)-graphene oxide system for thiophene polymerization: a new strategy, a new material. RSC Advances. 2016;6(30):25577-83.

10. Luan J, Wang S, Hu Z, Zhang L. Synthesis Techniques, Properties and Applications of Polymer Nanocomposites. Current Organic Synthesis. 2012;9(1):114-36.

11. Bernabò M, Pucci A, Ramanitra HH, Ruggeri G. Polymer Nanocomposites Containing Anisotropic Metal Nanostructures as Internal Strain Indicators. Materials. 2010;3(2):1461-77.

12. Zhao L, Gao M, Yue W, Jiang Y, Wang Y, Ren Y, et al. Sandwich-Structured Graphene-Fe3O4@Carbon Nanocomposites for High-Performance Lithium-Ion Batteries. ACS Applied Materials & Interfaces. 2015;7(18):9709-15.

13. Han K, Shen J, Hayner CM, Ye H, Kung MC, Kung HH. Li2S-reduced graphene oxide nanocomposites as cathode material for lithium sulfur batteries. Journal of Power Sources. 2014;251:331-7.

14. Arunachalam S, Battisti MG, Vijayakumar CT, Friesenbichler W. Cover Picture: Macromol. Mater. Eng. 10/2015. Macromolecular Materials and Engineering. 2015;300(10):949-.

15. Sharma S, Singh S, Khare N. Synthesis of polyaniline/CdS (nanoflowers and nanorods) nanocomposites: a comparative study towards enhanced photocatalytic activity for degradation of organic dye. Colloid and Polymer Science. 2016;294(5):917-26.

16. I. Nandapure B, B. Kondawar S, Y. Salunkhe M, I. Nandapure A. Magnetic And Transport Properties Of Conducting polyaniline/nickel Oxide Nanocomposites. Advanced Materials Letters. 2013;4(2):134-40.

17. Seyedzavar Z, Babazadeh M. Preparation of Novel Nanocomposites of Polythiophene with SnO2byIn SituChemical Polymerization Method and Evaluation of their Physical Properties. Synthesis and Reactivity in Inorganic, Metal-Organic, and Nano-Metal Chemistry. 2015;46(3):389-93.

18. Babazadeh M, Zalloi F, Olad A. Fabrication of Conductive Polyaniline Nanocomposites Based on Silica Nanoparticles viaIn-SituChemical Oxidative Polymerization Technique. Synthesis and Reactivity in Inorganic, Metal-Organic, and Nano-Metal Chemistry. 2013;45(1):86-91.

19. Islam S, Lakshmi GBVS, Siddiqui AM, Husain M, Zulfequar M. Synthesis, Electrical Conductivity, and Dielectric Behavior of Polyaniline/V2O5Composites. International Journal of Polymer Science. 2013;2013:1-7.

20. Jundale DM, Navale ST, Khuspe GD, Dalavi DS, Patil PS, Patil VB. Polyaniline-CuO hybrid nanocomposites: synthesis, structural, morphological, optical and electrical transport studies. Journal of Materials Science: Materials in Electronics. 2013;24(9):3526-35.

21. Wang X, Chen G, Zhang J. RETRACTED: Synthesis and characterization of novel Cu2O/PANI composite photocatalysts with enhanced photocatalytic activity and stability. Catalysis Communications. 2013;31:57-61.

22. Ballav N, Biswas M. Preparation and evaluation of a nanocomposite of polythiophene with Al2O3. Polymer International. 2003;52(1):179-84.

23. Batool A, Kanwal F, Imran M, Jamil T, Siddiqi SA. Synthesis of polypyrrole/zinc oxide composites and study of their structural, thermal and electrical properties. Synthetic Metals. 2012;161(23-24):2753-8.

24. Li B, Weng X, Wu G, Zhang Y, Lv X, Gu G. Synthesis of Fe 3 O 4 /polypyrrole/polyaniline nanocomposites by in-situ method and their electromagnetic absorbing properties. Journal of Saudi Chemical Society. 2017;21(4):466-72.

25. Babazadeh M. Conductive Polythiophene/Titanium Dioxide Nanocomposites: Synthesis and Investigation of Physical Properties. Asian Journal of Materials Chemistry. 2016;1(3-4):75-8.

26. Tompsett DA, Parker SC, Islam MS. Surface properties of α-MnO2: relevance to catalytic and supercapacitor behaviour. J Mater Chem A. 2014;2(37):15509-18.

27. Xu M, Wang H, Lei D, Qu D, Zhai Y, Wang Y. Removal of Pb(II) from aqueous solution by hydrous manganese dioxide: Adsorption behavior and mechanism. Journal of Environmental Sciences. 2013;25(3):479-86.

28. Rasul S, Suzuki S, Yamaguchi S, Miyayama M. Manganese oxide octahedral molecular sieves as insertion electrodes for rechargeable Mg batteries. Electrochimica Acta. 2013;110:247-52.

29. Alfaruqi MH, Islam S, Gim J, Song J, Kim S, Pham DT, et al. A high surface area tunnel-type α-MnO2 nanorod cathode by a simple solvent-free synthesis for rechargeable aqueous zinc-ion batteries. Chemical Physics Letters. 2016;650:64-8.

30. Yu P, Zhang X, Wang D, Wang L, Ma Y. Shape-Controlled Synthesis of 3D Hierarchical MnO2Nanostructures for Electrochemical Supercapacitors. Crystal Growth & Design. 2009;9(1):528-33.

31. Liu H, Tan L. A novel method for preparing lithium manganese oxide nanorods from nanorod precursor. Journal of Nanoparticle Research. 2009;12(1):301-5.

32. Brousse T, Toupin M, Dugas R, Athouël L, Crosnier O, Bélanger D. Crystalline MnO[sub 2] as Possible Alternatives to Amorphous Compounds in Electrochemical Supercapacitors. Journal of The Electrochemical Society. 2006;153(12):A2171.

33. Ni J, Lu W, Zhang L, Yue B, Shang X, Lv Y. Low-Temperature Synthesis of Monodisperse 3D Manganese Oxide Nanoflowers and Their Pseudocapacitance Properties. The Journal of Physical Chemistry C. 2008;113(1):54-60.

34. Li W, Liu Q, Sun Y, Sun J, Zou R, Li G, et al. MnO2 ultralong nanowires with better electrical conductivity and enhanced supercapacitor performances. Journal of Materials Chemistry. 2012;22(30):14864.

35. Wang X, Yuan A, Wang Y. Supercapacitive behaviors and their temperature dependence of sol-gel synthesized nanostructured manganese dioxide in lithium hydroxide electrolyte. Journal of Power Sources. 2007;172(2):1007-11.

36. Sangsefidi FS, Esmaeili-Zare M, Salavati-Niasari M. Hydrothermal synthesis and characterization of HgS nanostructures assisted by inorganic precursor. Journal of Industrial and Engineering Chemistry. 2015;28:197-201.

37. Sangsefidi FS, Mir N, Salavati-Niasari M. Hydrothermal synthesis and characterization of HgTe nanoribbons from [Hg(Salen)] as mercury source. Materials Science in Semiconductor Processing. 2014;27:500-6.

38. Sobhani A, Salavati-Niasari M. Hydrothermal synthesis, characterization, and magnetic properties of cubic MnSe 2 /Se nanocomposites material. Journal of Alloys and Compounds. 2014;617:93-101.

39. Wang X, Li Y. Rational synthesis of α-MnO2 single-crystal nanorods. Chemical Communications. 2002(7):764-5.

40. Mallakpour S, Abdolmaleki A, Tabebordbar H. Facile synthetic route for the preparation of PVC/α-MnO2-PVA nanocomposites: morphology, thermal, mechanical and Cd(II) adsorption properties. Polymer Bulletin. 2016;74(8):2957-73.

41. Niemi VM, Knuuttila P, Österholm JE, Korvola J.Polymerization of 3-alkylthiophenes with FeCl3. Polymer. 1992;33(7):1559-62.

42. Chanunpanich N, Ulman A, Strzhemechny YM, Schwarz SA, Dormicik J, Janke A, et al. Grafting polythiophene on polyethylene surfaces. Polymer International. 2003;52(1):172-8.

43. Masthead: (Adv. Mater. 43/2016). Adv Mater. 2016;28(43).

44. Tang N, Tian X, Yang C, Pi Z, Han Q. Facile synthesis of α-MnO2 nanorods for high-performance alkaline batteries. Journal of Physics and Chemistry of Solids. 2010;71(3):258-62.

45. Guan H, Xie J, Chen G, Wang Y. Facile synthesis of α-MnO2 nanorods at low temperature and their microwave absorption properties. Materials Chemistry and Physics. 2014;143(3):1061-8.

46. Sangsefidi FS, Sabet M, Salavati-Niasari M. Synthesis and characterization of ceria nanostructures with different morphologies via a simple thermal decompose method with different cerium complexes and investigation the photocatalytic activity. Journal of Materials Science: Materials in Electronics. 2016;27(8):8793-801.

47. Sangsefidi FS, Salavati-Niasari M, Esmaeili-Zare M. Hydrothermal method for synthesis of HgTe nanorods in presence of a novel precursor. Superlattices and Microstructures. 2013;62:1-11.

48. Safardoust-Hojaghan H, Shakouri-Arani M, Salavati-Niasari M. Structural and spectroscopic characterization of HgS nanoparticles prepared via simple microwave approach in presence of novel sulfuring agent. Transactions of Nonferrous Metals Society of China. 2016;26(3):759-66.

49. Sen P, De A, Chowdhury AD, Bandyopadhyay SK, Agnihotri N, Mukherjee M. Conducting polymer based manganese dioxide nanocomposite as supercapacitor. Electrochimica Acta. 2013;108:265-73.